

https://dspace.org/

Universal Crosstalk of Twisted Light in Random Media

David Bachmann; Asher Klug; Mathieu Isoard; Vyacheslav Shatokhin; Giacomo Sorelli ...

AMER PHYSICAL SOC
https://hdl.handle.net/10539/40654
WOS

Downloaded from a DSpace repository. https://dspace.org/

Universal Crosstalk of Twisted Light in Random Media

David Bachmann,[1,*] Asher Klug,[2] Mathieu Isoard,[1,†] Vyacheslav Shatokhin,[1,3] Giacomo Sorelli,[4,‡] Andreas Buchleitner,[1,3] and Andrew Forbes[2]

[1]*Physikalisches Institut, Albert-Ludwigs-Universität Freiburg, Hermann-Herder-Straße 3, D-79104 Freiburg, Germany*
[2]*School of Physics, University of the Witwatersrand, Private Bag 3, Johannesburg 2050, South Africa*
[3]*EUCOR Centre for Quantum Science and Quantum Computing, Albert-Ludwigs-Universität Freiburg, Hermann-Herder-Straße 3, D-79104 Freiburg, Germany*
[4]*Laboratoire Kastler Brossel, Sorbonne Université, ENS-Université PSL, Collège de France, CNRS; 4 place Jussieu, F-75252 Paris, France*

(Received 24 June 2022; accepted 12 December 2023; published 5 February 2024)

Structured light offers wider bandwidths and higher security for communication. However, propagation through complex random media, such as the Earth's atmosphere, typically induces intermodal crosstalk. We show numerically and experimentally that coupling of photonic orbital angular momentum modes is governed by a *universal* function of a single parameter: the ratio between the random medium's and the beam's transverse correlation lengths, even in the regime of pronounced intensity fluctuations.

DOI: 10.1103/PhysRevLett.132.063801

Introduction.—Optical communication strives to answer the growing demand of high-bandwidth links [1–3]. In particular, photonic spatial degrees of freedom such as *orbital angular momentum* (OAM) offer an unbounded Hilbert space to encode information, and provide intrinsic support for quantum key or entanglement distribution protocols [4–7], which with high-dimensional multiplexing enables greater channel capacities [8] and enhanced security [9]. While communication based on such *twisted photons* was successfully demonstrated for tabletop [10], indoor [11], and short outdoor [12] channels, transport of photonic OAM through *complex random media*, e.g., the atmosphere [13–15], water [16,17], or multimode fiber [3,18], remains challenging: stochastic fluctuations of the underlying media's refractive index induce phase distortions as well as intensity fluctuations upon propagation, leading to transmission losses and power transfer from information encoding modes to others—*intermodal crosstalk*—that hinders reliable identification of the input modes [19,20]. Hence, for a successful optical communication in complex random media we need to better understand intermodal crosstalk therein.

To that end, we consider OAM-carrying Laguerre-Gaussian (LG) modes, which are most commonly used for classical and quantum communication [1,3–7,10–22], as well as Bessel-Gaussian (BG) modes [23,24]. Information is typically encoded into the mode's OAM associated with the azimuthal index $\ell \in \mathbb{Z}$ [25]; in addition, the transverse amplitude distribution furnishes another degree of freedom characterized for LG [26,27] and BG [28] modes, respectively, by the discrete radial index $p \in \mathbb{N}_0$ and the continuous radial wave number $\beta \in \mathbb{R}^+$.

Their rich transverse intensity structures bring about various applications of twisted photons. For example, LG modes with $p = 0$ have the minimal space-bandwidth product and are usually employed in OAM-multiplexed systems [29]. Furthermore, the doughnutlike intensity distribution of such modes is relatively robust under perturbations [21,22]. On the other hand, LG modes with $p > 0$ allow for a substantial increase of the bandwidth capacity [30]. As for BG modes, they are promising due to their self-healing [31] and resilience [24,32] properties.

In this Letter, we show that twisted photons, i.e., LG and BG modes, exhibit a universal dependence of the crosstalk between modes with opposite OAM governed by the transverse length scale ratio of the beam and medium.

The model.—We consider transverse optical modes $\psi(\mathbf{r})$ arising within the paraxial approximation as solutions of the *parabolic wave equation* describing free diffraction [33]. Twisted light modes are cylindrically symmetric solutions of this equation [34]. They feature distinct phase and intensity profiles that may be characterized by the transverse *correlation length* ξ [35] and by their ℓ times intertwined helical phase fronts along the propagation axis z, as illustrated in Fig. 1(a).

However, photonic phase fronts are fragile under inherent refractive index fluctuations of the atmosphere or of other complex media. Here, we consider the propagation of a monochromatic laser beam through clear atmospheric channels, or through nonabsorbing Gaussian media. In either case, the typical size of refractive index inhomogeneities is much larger than the laser wavelength, so that wave scattering is mainly in the forward direction [33,36]. We choose the beam's wavelength to match the infrared transparency window of atmospheric turbulence [33], where wave attenuation due to absorption and multiple scattering by molecules and aerosols over propagation

 © 2024 American Physical Society

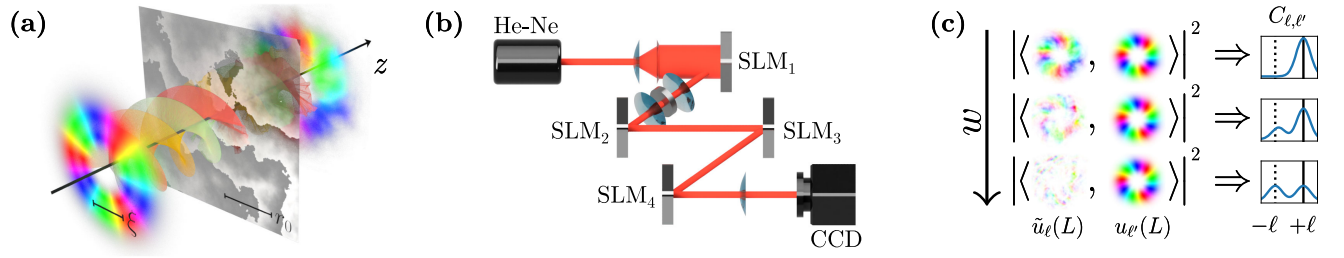


FIG. 1. (a) Incident $\mathrm{LG}_{p=0}^{\ell=3}$ beam with transverse correlation length ξ propagating through a random medium represented by a phase screen with correlation length r_0. (b) Experimental implementation of the split-step method via spatial light modulators (SLMs). (c) Qualitative illustration of crosstalk $C_{\ell,\ell'}$ of an incident $\mathrm{LG}_{p=0}^{\ell=3}$ mode, after propagation through a random medium to $z = L$, and of the vacuum-propagated $\mathrm{LG}_{p=0}^{\ell'}(z = L)$ modes, for increasing distortion strength $w = w_0/r_0$ from top to bottom. Original and opposed OAM, i.e., $\pm\ell$, are indicated by the solid and dashed black lines, respectively.

distances of a few kilometers is negligible [33,37]. In other words, our propagation distance L in the atmosphere is much shorter than the light's mean free path l [37,38], and the same regime is assumed for the Gaussian medium. The beam's remaining sensitivity to refractive index fluctuations is modeled by the *stochastic* parabolic equation, which incorporates random noise induced by the medium [33,39]. To find its solution, we employ the *split-step method* [40,41], which relies on segmenting the entire propagation path into discrete, medium-induced phase modulations, i.e., *phase screens* [see Fig. 1(a)] interconnected by free diffraction [40,42,43].

The phase screens incorporate the medium's transverse correlation length. For atmospheric *Kolmogorov turbulence* this characteristic length scale is known as the *Fried parameter* r_0 [33]; the ratio $w \coloneqq w_0/r_0$, with the *beam waist* w_0, quantifies the resulting *distortion strength*. Similarly, the *Rytov variance* σ_R^2 quantifies intensity fluctuations and distinguishes between *weak scintillation* $\sigma_R^2 < 1$ and *strong scintillation* $\sigma_R^2 \geq 1$ [36]. We ensure that every propagation segment satisfies $\sigma_R^2 < 1$. Furthermore, we represent more general random media by *Gaussian noise* based on normally distributed block matrices with block size r_0, independently altering both amplitude and phase of given transverse modes, where the block size r_0 mimics the correlation length of Kolmogorov turbulence. In this case, we suppress systematic anisotropies, e.g., due to distinct lengths of a block's side and diagonal, by randomly shifting and rotating the resulting noise grid within the transverse plane. Examples of a perturbed LG beam are shown in Fig. 2, where we distinguish three regimes of distortion: weak, moderate, and strong, quantified by $w < 1$, $w \approx 1$, and $w < 1$, respectively.

To benchmark our theoretical description, we experimentally realize a turbulent link by downscaling realistic channels to tabletop dimensions [44]. The setup, shown in Fig. 1(b), allows to experimentally simulate propagation through weak to strong scintillation. The salient elements are divided into three stages. In the generation stage, a He-Ne laser beam is expanded and collimated before being directed onto a reflective *spatial light modulator* (SLM_1) which generates the desired source mode. This mode then enters the distorting section of the setup where it passes through a random medium implemented by a two stage split-step propagation, with phase shifts programmed to SLM_2 and SLM_3, each followed by 1 m of free diffraction. This 2 m laboratory system maps to a $L = 200$ m real-world channel with Rytov variances of up to $\sigma_R^2 \approx 1.8$, matching the numerically investigated conditions. In the final stage, the modal decomposition is performed optically [45] with the aid of a match filter programmed to SLM_4 and a Fourier transforming lens, with the on-axis intensity measured with a camera (CCD detector).

Crosstalk among distorted modes.—The probability of identifying a source mode's original OAM ℓ after propagation as ℓ' is quantified via the *crosstalk matrix*

$$C_{\ell,\ell'}(L) \coloneqq |\langle \tilde{u}_\ell(L), u_{\ell'}(L)\rangle|^2, \tag{1}$$

where $\tilde{u}_\ell(L)$ and $u_{\ell'}(L)$ are complex modes [46] propagated across a random medium and through a vacuum channel each of length L, respectively, and $\langle\cdot,\cdot\rangle$ denotes the standard scalar product in the transverse space at $z = L$ [47]. The distorted modes $\tilde{u}_\ell(L)$ are connected to the incident modes u_ℓ by the transmission operator $T(L)$, which approximates the medium's scattering matrix [48] whenever wave reflection is neglected. Although geometric truncation due to finite size apertures induces nonunitarity of $T(L)$, its eigenvalues in weak turbulence exhibit the bimodal distribution [49] that characterizes complex scattering media [48]. Accordingly, the crosstalk matrix can be interpreted as the square modulus of the elements of the transmission operator's matrix representation in the bases of the incident modes and their vacuum-propagated images.

Consequently, higher transmission fidelities correspond to weaker crosstalk, i.e., to matrices $C_{\ell,\ell'}(L)$ with prevailing diagonals. Figure 1(c) sketches the crosstalk amplitudes for a fixed source mode $\mathrm{LG}_{p=0}^{\ell=3}$ after propagation through a channel of length L, for three distortion regimes quantified

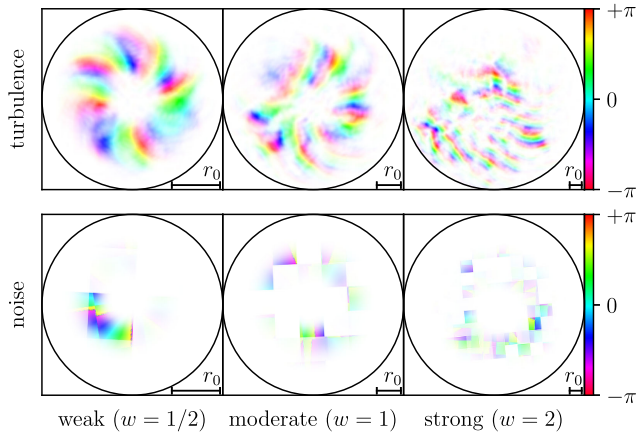


FIG. 2. Intensity-weighted transverse phase profiles of an incident $\mathrm{LG}_{p=0}^{\ell=5}$ mode, after propagation through Kolmogorov turbulence (top), or through Gaussian noise (bottom), for three different distortion strengths $w = 1/2$, 1, 2, corresponding to $\sigma_R^2 = 0.24$, 0.76, 2.42 from left to right.

by w. As observed previously [50], under weak distortion (top row) the detection probability of the original OAM $\ell = 3$ (solid black line) is highest and crosstalk is limited to neighboring modes. In contrast, under strong distortion [see bottom row of Fig. 1(c)], we find a $\pm\ell$-symmetric distribution of the crosstalk amplitudes with separate maxima close to $\pm\ell$ (black lines). In this case, the mode's phase front is destroyed, while its amplitude—which is on average independent of the sign of OAM—partially survives. Finally, the moderate distortion regime [see center row of Fig. 1(c)] is of particular interest: it represents the transition between rather faithful OAM transmission (top row) and dominant phase destruction (bottom row). Both, the beam's amplitude and phase profiles are altered, but neither is completely destroyed.

To elucidate the origin of the disorder-induced crosstalk between OAM modes, we decompose the incident LG_p^ℓ, yielding $\tilde{u}_\ell(L)$ in Eq. (1) after transmission through moderate, $w = 1$, disorder at $z = L$, into the vacuum-propagated LG modes by setting $u_{\ell'}(L) = \mathrm{LG}_p^{\ell'}(z = L)$ in Eq. (1) as illustrated for $p = 0$ in Fig. 3. Furthermore, we quantify the channel's imprint on the transmitted beam's phase and intensity profile alone by setting $u_{\ell'}(L)$ to $\arg[\mathrm{LG}_p^{\ell'}(z = L)]$ and $|\mathrm{LG}_p^{\ell'}(z = L)|$ in Eq. (1), respectively [see left and right columns of Figs. 3(a) and 3(b)]. Note that, in general, random media also induce coupling to modes with $p' \neq p$, but the prescribed projection onto individual radial indices is common in communication scenarios [51,52], and required when finite-size apertures geometrically truncate modes with larger p, or if both, p and ℓ, are used for information encoding.

The phase profile [see top left plots in Figs. 3(a) and 3(b)], of the crosstalk matrix concentrates about the diagonal, which manifests the prevailing coherent coupling of modes with matching OAM, i.e., $\ell' = \ell$, confirming previous findings [50]. Furthermore, the diagonal's broadening attests to disorder-induced coupling among modes with different OAM, i.e., $\ell' \neq \ell$. In contrast, when projecting onto the amplitude profiles [see top right plots in Figs. 3(a) and 3(b)], crosstalk matrices exhibit pronounced, symmetric diagonal and *antidiagonal* structures. Their symmetry is expected because the amplitude of LG modes is independent of the sign of OAM, and their shape is very suggestive when considering the projection onto LG modes [see top middle

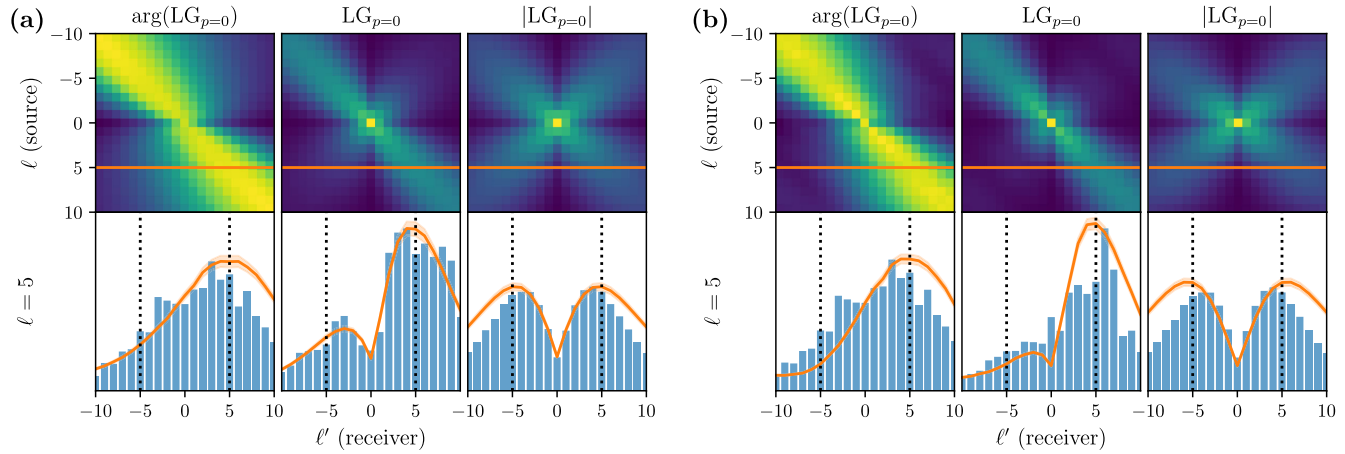


FIG. 3. Numerically obtained average (2500 realizations) crosstalk matrices in moderate ($w = 1$) Kolmogorov turbulence (a) and Gaussian noise (b). The crosstalk matrices (top) are obtained when projecting the image $\tilde{u}_\ell(L)$ of the incident mode $\mathrm{LG}_{p=0}^\ell$, onto vacuum-propagated modes $u_{\ell'}(L) = \mathrm{LG}_{p=0}^{\ell'}(z = L)$ in the middle columns, according to Eq. (1). Left and right columns represent the beam's phase and intensity profiles' modifications quantified by substitution of $\arg[\mathrm{LG}_{p=0}^{\ell'}(z = L)]$ and $|\mathrm{LG}_{p=0}^{\ell'}|$ for $u_{\ell'}(L)$ in Eq. (1), respectively. Rows $C_{\ell=5,\ell'}$ (bottom) depict numerical (orange curve, error bands give 1 standard deviation) as well as experimental results (blue bars, 60 realizations). The crosstalk matrices are normalized such that $\sum_{\ell,\ell'=-10}^{10} C_{\ell,\ell'} = 1$.

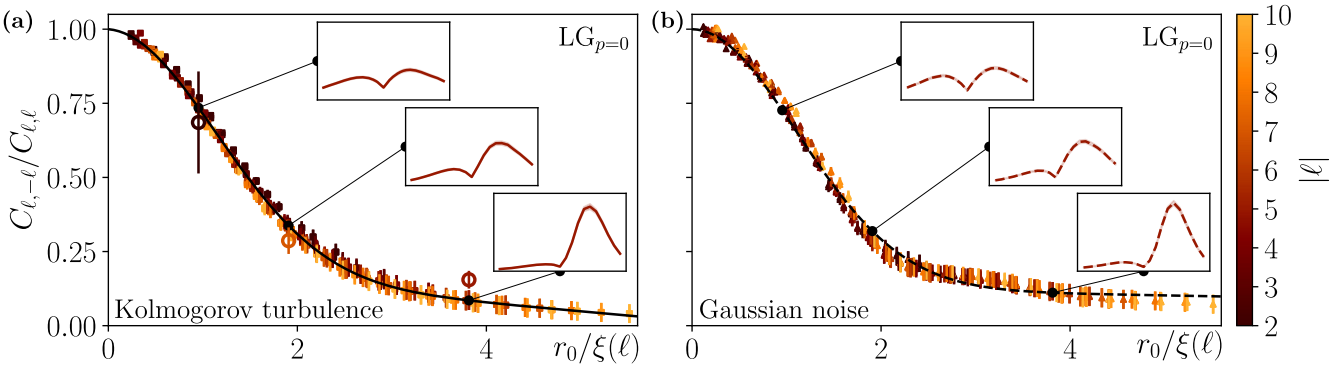


FIG. 4. Ratio of average (2500 realizations) crosstalk between two OAM-opposed (i.e., ℓ and $-\ell$) modes propagated through numerically simulated Kolmogorov turbulence (a) and Gaussian noise (b) versus the ratio of the medium's and beam's transverse coherence lengths for a range of azimuthal indices $|\ell|$. The incident $\mathrm{LG}^{\ell}_{p=0}$ were projected onto $\mathrm{LG}^{\mp\ell}_{p=0}(z=L)$ at the receiver side. The emerging universal curve is fitted with a Gaussian (black curves) with parameters in [58]. Circles with error bars in (a) represent experimentally measured average (60 realizations) crosstalk in Kolmogorov turbulence. Insets illustrate rows at $\ell=5$ of corresponding crosstalk matrices (same axes as in Fig. 3). Error bands or bars give 1 standard deviation.

plots in Figs. 3(a) and 3(b). Coherent coupling of neighboring modes, due to matching OAM phase is combined with the antidiagonal crosstalk originating from amplitude overlap, leading to the presence of damped antidiagonal elements in agreement with Ref. [52].

The lower row of Fig. 3 compares experimental measurements (blue bars) with numerical results (orange curves) in form of crosstalk matrix rows that describe the detection probabilities of various ℓ' when transmitting $\ell=5$, cf. orange lines in the upper plots. Experimental results qualitatively agree with numerical results, and their systematic underestimation for larger ℓ' originates from the receiving aperture damping the overall transmission of these correspondingly wider modes [33]. In the bottom middle plots of Figs. 3(a) and 3(b), i.e., when projecting onto full LG modes, we observe an *asymmetric doublet* whose second diminished peak is systematically shifted toward the center. While crosstalk between $\pm\ell$ is still amplified, this behavior further highlights that we do not observe direct $\pm\ell$ coupling of LG modes but rather a tradeoff between destruction of OAM-preserving phase and surviving symmetric amplitude.

We note that *antidiagonal*, i.e., $\pm\ell$, crosstalk becomes weaker for larger $|\ell|$, cf. fading of antidiagonals in the top middle plots of Figs. 3(a) and 3(b). This observation is consistent with well-known results that entangled photonic OAM qubit states with opposite ℓ become more robust in turbulence as $|\ell|$ increases [53]. Careful study of LG modes [35] within the weak scintillation regime attributed this enhanced robustness to the finer transverse spatial structure of such photons characterized by their analytically given phase correlation length ξ. The latter gives the average distance between two points in the transverse profile of LG beams with a phase difference of $\pi/2$ [35,54].

Because of its ubiquity in communication protocols [11,15,35,53,55,56], we further explore the antidiagonal crosstalk for a range of distortion strengths w and azimuthal indices ℓ of incident OAM modes. To this end, we investigate the ratio between antidiagonal and diagonal crosstalk, i.e., $C_{\ell,-\ell}$ over $C_{\ell,\ell}$. For LG modes, this ratio is plotted in Fig. 4, versus the medium's transverse correlation length r_0 normalized by ξ for Kolmogorov turbulence and Gaussian noise. Further modes are considered in the Supplemental Material [47]. Remarkably, the rescaling of r_0 collapses the data onto a *universal*, i.e., ℓ-independent, crosstalk curve, even in the regime of strong scintillation. Given the analogy between optical wave transmission and electronic transport [57], this behavior is reminiscent of the *universal conductance fluctuations* observed for electrons in solid state physics [48], where scattering properties are a universal function of L/l. However, the latter universality occurs in the diffusive regime, $L/l \gg 1$, which is opposite to the one here considered.

To ease the comparison and to highlight the universality, the data points were fitted by a Gaussian [58] with decaying offset, to mimic the slow systematic noise reduction with decreasing distortion strength. It is notable that the two considered, i.e., Kolmogorov and Gaussian, media, albeit fundamentally different, result in a very similar crosstalk decay, which is attributed to their similar transverse length scale.

The crosstalk ratio in Fig. 4 reflects the crossover from symmetric doublets in strong distortion, where OAM-encoding phase information is destroyed, to dominant direct ℓ coupling in weak distortion. Moreover, the numerical results are in quantitative agreement with experimental data for Kolmogorov turbulence [see circles in Fig. 4(a)] in the moderate and strong turbulence regime; the measurement for weak turbulence [see rightmost circle] shows a systematic offset due to the decreased signal-to-noise ratio of the diminished antidiagonal crosstalk in this case. The universality of crosstalk for both Kolmogorov

turbulence and generic Gaussian noise suggests that such agreement can also be expected for other random media.

Discussion.—The universal dependence of crosstalk amplitudes between modes of opposite OAM on the rescaled Fried parameter was previously predicted in the regime of weak scintillation, for Kolmogorov [35] and non-Kolmogorov turbulence [56] alike, as well as under deterministic perturbation of twisted photons by angular apertures [59]. Moreover, it was established that in this regime bipartite entanglement of photonic qubit states with opposite OAM depends on the same parameters as crosstalk and, hence, exhibits universal behavior as well [35,56,59]. However, entanglement of twisted photons depends on intensity fluctuations [60] and this sensitivity renders rescaling into a universal entanglement evolution impossible under strong scintillation. Our present theoretical and experimental results show that *crosstalk* among structured light modes is nonetheless universal beyond weak scintillation conditions. Importantly, only the characteristic transverse correlation length of the medium-induced errors needs be known to understand the impact of modal scattering on twisted light modes, with clear impact in imaging and communication through noisy channels. This result in particular implies that the ubiquitous superposition of $\pm\ell$ [11,15,35,53,55,56], is far from an optimal choice of encoding information.

Conclusion.—In this Letter, we have studied the crosstalk of twisted photons in Kolmogorov turbulence and Gaussian noise. In both cases, we have numerically as well as experimentally confirmed pronounced crosstalk among LG modes of opposed OAM. Instead of originating from direct OAM cross coupling, this behavior was identified as a tradeoff effect between matching intensity patterns and destroyed phase information. Moreover, we have uncovered a universal crosstalk decay complying with experimental measurements by setting the random media's transverse correlation length into relation with the beam's phase structure. We have established that the universality holds for LG modes with different radial indices, that is, with different transverse amplitude distributions, as well as for BG modes with different beam waists [47]. We therefore envisage a similar behavior for other sets of OAM modes upon a suitable generalization of the phase correlation length [35,47].

Our results may lead to novel venues for communication. In particular, optimizing the beam's transverse correlation length for given distortion strengths will diminish the crosstalk, irrespective of the precise nature of the underlying random medium itself. As we have demonstrated, this can be achieved by suitable choice of ℓ or p (β) for LG (BG), or, due to the scaling properties of LG and BG modes, by adapting the beam waist w_0.

D. B. acknowledges financial support by the Studienstiftung des deutschen Volkes. The authors acknowledge support by the state of Baden-Württemberg through bwHPC and the German Research Foundation (DFG) through Grant No. INST 40/575-1 FUGG (JUSTUS 2 cluster). G. S. acknowledges partial funding by French ANR (ANR-19-ASTR0020-01). V. S. and A. B. acknowledge partial funding and support through the Strategiefonds der Albert-Ludwigs-Universität Freiburg and the Georg H. Endress Stiftung.

*Corresponding author: david.bachmann@physik.uni-freiburg.de
†Present address: Laboratoire Kastler Brossel, Sorbonne Université, ENS-Université PSL, Collège de France, CNRS, 4 place Jussieu, F-75252 Paris, France.
‡Present address: Fraunhofer IOSB, Ettlingen, Fraunhofer Institute of Optronics, System Technologies and Image Exploitation, Gutleuthausstraße 1, D-76275 Ettlingen, Germany.

[1] M. P. J. Lavery *et al.*, Tackling Africa's digital divide, Nat. Photonics **12**, 249 (2018).
[2] B. J. Puttnam, G. Rademacher, and R. S. Luís, Space-division multiplexing for optical fiber communications, Optica **8**, 1186 (2021).
[3] Y. Zhou, B. Braverman, A. Fyffe, R. Zhang, J. Zhao, A. E. Willner, Z. Shi, and R. W. Boyd, High-fidelity spatial mode transmission through a 1-km-long multimode fiber via vectorial time reversal, Nat. Commun. **12**, 1866 (2021).
[4] B.-J. Pors, F. Miatto, G. W. 't Hooft, E. R. Eliel, and J. P. Woerdman, High-dimensional entanglement with orbital-angular-momentum states of light, J. Opt. **13**, 064008 (2011).
[5] J. Leach, E. Bolduc, D. J. Gauthier, and R. W. Boyd, Secure information capacity of photons entangled in many dimensions, Phys. Rev. A **85**, 060304(R) (2012).
[6] R. Fickler, R. Lapkiewicz, W. N. Plick, M. Krenn, C. Schaeff, S. Ramelow, and A. Zeilinger, Quantum entanglement of high angular momenta, Science **338**, 640 (2012).
[7] E. Otte, I. Nape, C. Rosales-Guzmán, C. Denz, A. Forbes, and B. Ndagano, High-dimensional cryptography with spatial modes of light: tutorial, J. Opt. Soc. Am. B **37**, A309 (2020).
[8] J. Wang, J.-Y. Yang, I. M. Fazal, N. Ahmed, Y. Yan, H. Huang, Y. Ren, Y. Yue, S. Dolinar, M. Tur, and A. E. Willner, Terabit free-space data transmission employing orbital angular momentum multiplexing, Nat. Photonics **6**, 488 (2012).
[9] S. Gröblacher, T. Jennewein, A. Vaziri, G. Weihs, and A. Zeilinger, Experimental quantum cryptography with qutrits, New J. Phys. **8**, 75 (2006).
[10] M. Mirhosseini, O. S. Magaña-Loaiza, M. N. O'Sullivan, B. Rodenburg, M. Malik, M. P. J. Lavery, M. J. Padgett, D. J. Gauthier, and R. W. Boyd, High-dimensional quantum cryptography with twisted light, New J. Phys. **17**, 033033 (2015).
[11] G. Vallone, V. D'Ambrosio, A. Sponselli, S. Slussarenko, L. Marrucci, F. Sciarrino, and P. Villoresi, Free-space quantum key distribution by rotation-invariant twisted photons, Phys. Rev. Lett. **113**, 060503 (2014).

[12] A. Sit, F. Bouchard, R. Fickler, J. Gagnon-Bischoff, H. Larocque, K. Heshami, D. Elser, C. Peuntinger, K. Günthner, B. Heim, C. Marquardt, G. Leuchs, R. W. Boyd, and E. Karimi, High-dimensional intracity quantum cryptography with structured photons, Optica **4**, 1006 (2017).

[13] B.-J. Pors, C. H. Monken, E. R. Eliel, and J. P. Woerdman, Transport of orbital-angular-momentum entanglement through a turbulent atmosphere, Opt. Express **19**, 6671 (2011).

[14] M. Malik, M. O'Sullivan, B. Rodenburg, M. Mirhosseini, J. Leach, M. P. J. Lavery, M. J. Padgett, and R. W. Boyd, Influence of atmospheric turbulence on optical communications using orbital angular momentum for encoding, Opt. Express **20**, 13195 (2012).

[15] A. Hamadou Ibrahim, F. S. Roux, M. McLaren, T. Konrad, and A. Forbes, Orbital-angular-momentum entanglement in turbulence, Phys. Rev. A **88**, 012312 (2013).

[16] Y. Ren, L. Li, Z. Wang, S. M. Kamali, E. Arbabi, A. Arbabi, Z. Zhao, G. Xie, Y. Cao, N. Ahmed, Y. Yan, C. Liu, A. J. Willner, S. Ashrafi, M. Tur, A. Faraon, and A. E. Willner, Orbital angular momentum-based space division multiplexing for high-capacity underwater optical communications, Sci. Rep. **6**, 33306 (2016).

[17] F. Bouchard, A. Sit, F. Hufnagel, A. Abbas, Y. Zhang, K. Heshami, R. Fickler, C. Marquardt, G. Leuchs, R. w. Boyd, and E. Karimi, Quantum cryptography with twisted photons through an outdoor underwater channel, Opt. Express **26**, 22563 (2018).

[18] M. W. Matthès, Y. Bromberg, J. de Rosny, and S. M. Popoff, Learning and Avoiding Disorder in Multimode Fibers, Phys. Rev. X **11**, 021060 (2021).

[19] C. Paterson, Atmospheric turbulence and orbital angular momentum of single photons for optical communication, Phys. Rev. Lett. **94**, 153901 (2005).

[20] M. A. Cox, N. Mphuthi, I. Nape, N. Mashaba, L. Cheng, and A. Forbes, Structured light in turbulence, IEEE J. Sel. Top. Quantum Electron. **27**, 1 (2021).

[21] M. Krenn, J. Handsteiner, M. Fink, R. Fickler, R. Ursin, M. Malik, and A. Zeilinger, Twisted light transmission over 143 km, Proc. Natl. Acad. Sci. U.S.A. **113**, 13648 (2016).

[22] M. P. J. Lavery, C. Peuntinger, K. Günthner, P. Banzer, D. Elser, R. W. Boyd, M. J. Padgett, C. Marquardt, and G. Leuchs, Free-space propagation of high-dimensional structured optical fields in an urban environment, Sci. Adv. **3**, e1700552 (2017).

[23] M. McLaren, M. Agnew, J. Leach, F. S. Roux, M. J. Padgett, R. W. Boyd, and A. Forbes, Entangled Bessel-Gaussian beams, Opt. Express **20**, 23589 (2012).

[24] T. Doster and A. T. Watnik, Laguerre–Gauss and Bessel–Gauss beams propagation through turbulence: analysis of channel efficiency, Appl. Opt. **55**, 10239 (2016).

[25] L. Allen, M. W. Beijersbergen, R. J. C. Spreeuw, and J. P. Woerdman, Orbital angular momentum of light and the transformation of Laguerre-Gaussian laser modes, Phys. Rev. A **45**, 8185 (1992).

[26] E. Karimi, R. W. Boyd, P. de la Hoz, H. de Guise, J. Řeháček, Z. Hradil, A. Aiello, G. Leuchs, and L. L. Sánchez-Soto, Radial quantum number of Laguerre-Gauss modes, Phys. Rev. A **89**, 063813 (2014).

[27] Y. Zhou, M. Mirhosseini, D. Fu, J. Zhao, S. M. Hashemi Rafsanjani, A. E. Willner, and R. W. Boyd, Sorting photons by radial quantum number, Phys. Rev. Lett. **119**, 263602 (2017).

[28] F. Gori, G. Guattari, and C. Padovani, Bessel-Gauss beams, Opt. Commun. **64**, 491 (1987).

[29] N. Zhao, X. Li, G. Li, and J. M. Kahn, Capacity limits of spatially multiplexed free-space communication, Nat. Photonics **9**, 822 (2015).

[30] A. Trichili, C. Rosales-Guzmán, A. Dudley, B. Ndagano, A. Ben Salem, M. Zghal, and A. Forbes, Optical communication beyond orbital angular momentum, Sci. Rep. **6**, 27674 (2016).

[31] M. McLaren, T. Mhlanga, M. J. Padgett, F. S. Roux, and A. Forbes, Self-healing of quantum entanglement after an obstruction, Nat. Commun. **5**, 3248 (2014).

[32] G. Sorelli, V. N. Shatokhin, F. S. Roux, and A. Buchleitner, Diffraction-induced entanglement loss of orbital-angular-momentum states, Phys. Rev. A **97**, 013849 (2018).

[33] L. Andrews, *Laser Beam Propagation through Random Media* (SPIE, Bellingham, 2005).

[34] A. Forbes, M. de Oliveira, and M. R. Dennis, Structured light, Nat. Photonics **15**, 253 (2021).

[35] N. D. Leonhard, V. N. Shatokhin, and A. Buchleitner, Universal entanglement decay of photonic-orbital-angular-momentum qubit states in atmospheric turbulence, Phys. Rev. A **91**, 012345 (2015).

[36] A. Ishimaru, *Wave Propagation and Scattering in Random Media* (Academic Press, New York, 1978).

[37] At a wavelength of $\lambda = 1550$ nm, about 99% of the incident power is transmitted over a distance of 1 km [33]. From the Lambert-Beer law, this corresponds to the mean free path $l \simeq 100$ km [38,48].

[38] R. Carminati and J. C. Schotland, *Principles of Scattering and Transport of Light* (Cambridge University Press, Cambridge, England, 2021).

[39] M. Segev, Y. Silberberg, and D. N. Christodoulides, Anderson localization of light, Nat. Photonics **7**, 197 (2013).

[40] J. Schmidt, *Numerical Simulation of Optical Wave Propagation with Examples in MATLAB* (SPIE, Bellingham, 2010).

[41] M. R. Chatterjee and F. H. A. Mohamed, Split-step approach to electromagnetic propagation through atmospheric turbulence using the modified von Karman spectrum and planar apertures, Opt. Eng. **53**, 126107 (2014).

[42] M. Born, *Principles of Optics: Electromagnetic Theory of Propagation, Interference and Diffraction of Light* (Cambridge University Press, New York, 1999).

[43] J. Goodman, *Introduction to Fourier Optics* (Roberts & Co, Englewood, 2005).

[44] B. Rodenburg, M. Mirhosseini, M. Malik, O. S. Magaña-Loaiza, M. Yanakas, L. Maher, N. K. Steinhoff, G. A. Tyler, and R. W. Boyd, Simulating thick atmospheric turbulence in the lab with application to orbital angular momentum communication, New J. Phys. **16**, 033020 (2014).

[45] J. Pinnell, I. Nape, B. Sephton, M. A. Cox, V. Rodríguez-Fajardo, and A. Forbes, Modal analysis of structured light with spatial light modulators: a practical tutorial, J. Opt. Soc. Am. A **37**, C146 (2020).

[46] The full mode functions read $u_{p=0,\ell}(\rho, \varphi, z = L)$, where the radial indices $p = 0$ and the transverse coordinates ρ, φ were suppressed for brevity.

[47] See Supplemental Material at http://link.aps.org/supplemental/10.1103/PhysRevLett.132.063801 for higher order LG and BG modes.

[48] C. W. J. Beenakker, Random-matrix theory of quantum transport, Rev. Mod. Phys. **69**, 731 (1997).

[49] D. Bachmann, M. Isoard, V. Shatokhin, G. Sorelli, N. Treps, and A. Buchleitner, Highly transmitting modes of light in dynamic atmospheric turbulence, Phys. Rev. Lett. **130**, 073801 (2023).

[50] A. Klug, I. Nape, and A. Forbes, The orbital angular momentum of a turbulent atmosphere and its impact on propagating structured light fields, New J. Phys. **23**, 093012 (2021).

[51] F. Bouchard, N. H. Valencia, F. Brandt, R. Fickler, M. Huber, and M. Malik, Measuring azimuthal and radial modes of photons, Opt. Express **26**, 31925 (2018).

[52] G. Sorelli, N. Leonhard, V. N. Shatokhin, C. Reinlein, and A. Buchleitner, Entanglement protection of high-dimensional states by adaptive optics, New J. Phys. **21**, 023003 (2019).

[53] B. J. Smith and M. G. Raymer, Two-photon wave mechanics, Phys. Rev. A **74**, 062104 (2006).

[54] D. Yang, Z.-D. Hu, S. Wang, and Y. Zhu, Phase correlation arc and universal decay of entangled orbital angular momentum qubit states in atmospheric turbulence, Opt. Lett. **46**, 5461 (2021).

[55] B. Ndagano, B. Perez-Garcia, F. S. Roux, M. McLaren, C. Rosales-Guzman, Y. Zhang, O. Mouane, R. I. Hernandez-Aranda, T. Konrad, and A. Forbes, Characterizing quantum channels with non-separable states of classical light, Nat. Phys. **13**, 397 (2017).

[56] D. Bachmann, V. N. Shatokhin, and A. Buchleitner, Universal entanglement decay of photonic orbital angular momentum qubit states in atmospheric turbulence: an analytical treatment, J. Phys. A **52**, 405303 (2019).

[57] E. Akkermans and G. Montambaux, *Mesoscopic Physics of Electrons and Photons* (Cambridge University Press, Cambridge, UK, 2007).

[58] Fit of the form $f(x) = (1 - a)\exp[-\frac{1}{2}(x/b)^2] + a - cx$ with $a = 0.208 \pm 0.014$, $b = 1.687 \pm 0.012$, $c = 0.032 \pm 0.004$ for Kolmogorov turbulence and $a = 0.129 \pm 0.009$, $b = 1.644 \pm 0.007$, $c = 0.007 \pm 0.002$ for Gaussian noise.

[59] G. Sorelli, V. N. Shatokhin, and A. Buchleitner, Universal entanglement loss induced by angular uncertainty, J. Opt. **22**, 024002 (2020).

[60] F. S. Roux, T. Wellens, and V. N. Shatokhin, Entanglement evolution of twisted photons in strong atmospheric turbulence, Phys. Rev. A **92**, 012326 (2015).